Contents lists available at ScienceDirect

Materials Today Communications

journal homepage: www.elsevier.com/locate/mtcomm

Dentin remineralization induced by nanobioactive glass in association with RGDS peptide

Sainan Wang , Xuyan Sheng , Guibin Huang , Qiuju Li , Yanmei Dong *

Department of Cariology and Endodontology, Peking University School and Hospital of Stomatology, Beijing, 100081, China

ARTICLE INFO

ABSTRACT

The aim of this study was to investigate the binding ability of a arginine-glycine-aspartate-serine (RGDS) peptide to dentin and its effect on the dentin remineralization, dentin cohesive strength and intrafibrillar mineralization induced by nanobioactive glass (nBG). The demineralized dentin discs were treated with RGDS and/or nBG and then incubated in stimulated body fluid for 2 weeks. The results of scanning electron microscopy, energy-dispersive X-ray spectroscopy, X-ray diffraction and confocal laser scanning microscopy showed that RGDS could bind to dentin and promote the attachment of nBG. Compared to the nBG group, the RGDS + nBG group induced more apatite formation on the dentin surface and apatite rods inside the dentinal tubules. The results of transmission electron microscopy showed crystal lattice formation in the demineralized dentin matrix treated with nBG or RGDS + nBG, indicating the remineralization of dentin. The RGDS + nBG-treated dentin had the highest dentin cohesive strength in all groups. The self-assembled collagen fibrils exposed to RGDS + nBG exhibited intrafibrillar mineralization. In conclusion, RGDS promoted nBG-induced apatite formation and dentin collagen matrix remineralization, thus enhancing the dentin strength. The results lay a foundation for the wide application of RGDS and nBG in dentin erosion, dentin hypersensitivity, dentin bonding interface improvement, and regenerative dentistry.

1. Introduction

Dental diseases, such as caries and erosion, often cause the demineralization of dentin, the disintegration of collagen and the formation of hard tissue defects in the tooth. In addition, acidic chemical reagent etching as a part of restorative adhesive materials also results in dentin demineralization, and demineralized regions with incomplete resin infiltration are susceptible to collagen degradation, resulting in a reduction in bond strength [1]. Therefore, remineralization of demineralized dentin is important for controlling dental caries and improving dentin bonding stability [2–4]. Dentin consists of a collagen matrix and hydroxyapatite nanocrystals hierarchically deposited between (extrafibrillar) and within (intrafibrillar) collagen fibrils. Although intrafibrillar minerals account for only 25%–30% of the dentin mineral phase, they are the major contributors to the mechanical properties of dentin [5,6]. When dentin is remineralized by simple calcium phosphate precipitation on the lesion surface and the minerals do not infiltrate the collagen fibrils, it is not sufficient to ideally restore the mechanical properties [6,7]. The biomimetic remineralization strategy attempts to

achieve close bonding between mineral crystallites and the collagen matrix, especially intrafibrillar mineralization, which is very promising for the restoration of functional dentin [8].

Bioactive glass (BG) is a well-studied biomaterial with an indicated ability to induce hydroxyapatite (HA) formation and osteoinductive capacity. In the oral environment, BG treatment forms HA on the dentin surface [9], seals the dentinal tubules, reduces the permeability of the dentin, and thus, alleviates dentin sensitivity [10–12]. In recent years, BG has also been added as a filler in newly developed materials or in existing materials to improve their restorative and regenerative capacity [13,14]. Demineralized dentin treated with BG showed mineral and microhardness gains [15,16], but whether the remineralization that is formed is intrafibrillar mineralization or only extrafibrillar mineralization has not been well explored. Nanotechnology provides revolutionary ways for materials to meet new needs. Our previous study showed that dentin treated with nanoBG (nBG, with a particle size of approximately 20 nm) had the highest apatite formation quantity with the strongest acid resistance compared to dentin treated with microscale BG (with a particle size of 2–20 μm) and submicroscale BG (with a particle size of

---

* Corresponding author at: Peking University School and Hospital of Stomatology, 22 Zhongguancun Nandajie, Haidian district, Beijing, 100081, China.
E-mail address: kqdongyanmei@bjmu.edu.cn (Y. Dong).

approximately 500 nm) [17]. Thus, nBG is a suitable candidate for dentin remineralization.

In the biomineralization of dentin, noncollagenous proteins (NCPs), such as dentin matrix protein 1 (DMP1) and dentin phosphoproteins (DPP), have crucial roles in the initiation of mineral nucleation and crystal growth during the mineralization process [18,19]. Therefore, many researchers are focused on finding and developing strategies that mimic the functions of NCPs for biomimetic remineralization. Synthesized peptides, peptide-like polymers and oligopeptides that mimic the function of NCPs can improve dentin remineralization and mechanical strength [20–22]. In addition, charged polymers, such as polyacrylic acid and polyvinylphosphonic acid, are used as NCP analogs for intrafibrillar mineralization of dentin [23,24]. DPP and DMP1 are particularly rich in serine, aspartic acid and glutamic residues and contain a common short peptide sequence of arginine-glycine-aspartate (RGD) [19]. These amino acids contain large amounts of carboxyl structures, which have a strong binding ability to participate with calcium ions in dentin mineralization [25–27]. Therefore, the incorporation of RGD-serine (RGDS) peptide may be an effective method for improving biomimetic remineralization of demineralized dentin.

In this study, our hypothesis is that pretreatment with a RGDS peptide improves the dentin remineralization process in the presence of nBG.

2. Materials and methods

2.1. Sample preparation

Intact human third molars were collected with the approval of the Ethics Committee, and all patients provided informed consent. The obtained teeth were stored in distilled water containing 0.9 % NaCl at 4 °C. Dentin discs at the crown part of the teeth were cut at a thickness of 1 mm with a hard histotome (SP1600, Leica, Wetzlar, Germany). The dentinal tubules were aligned perpendicular to the specimen surface being treated. After removing the surrounding enamel with diamond burs, the dentin discs were divided into four parts. The dentin surfaces were wet ground using 600 grit silicone abrasive paper to increase their smoothness. The dentin discs were then immersed in 17 % ethylenediaminetetraacetic acid (EDTA) (pH = 7.4) at room temperature for 7 days with shaking, and the solution was changed on alternate days. In this way, completely demineralized dentin discs were obtained [17,28]. The discs were rinsed thoroughly with deionized water 3 times and randomly divided into four groups: the control group, RGDS group, nBG group, and RGDS + nBG group.

2.2. Bioactive glass/RGDS and treatment procedures

The nBG sol–gel particles with molar compositions of 58 % SiO_2, 33 % CaO and 9% P_2O_5 were prepared according to the procedure reported in previous work [29]. The nBG exhibited a spherical morphology with a particle size of approximately 20 nm (Fig. 1A,B) and was composed of large amounts of silicon (Si), some calcium (Ca), and phosphate (P) (Fig. 1C). The surface area of nBG was 63.545 ± 0.2 m^2/g. The nBG particles were labeled with rhodamine B [30]. Next, 10 mg of rhodamine B powder was dissolved in 10 mL of deionized water to prepare a 0.1 % rhodamine B solution. nBG particles were incubated in rhodamine B solution overnight and then washed with deionized water 3–5 times until the liquid supernatant became colorless. Rhodamine B-labeled nBG particles were obtained by freeze-drying. The nBG particles were mixed with deionized water to form an nBG suspension at 50 wt%; 0.05 g of nBG particles was suspended in 0.1 mL deionized water and vibrated under ultrasound for 1 min [17]. The acquired nBG suspension was used immediately after preparation. The dentin discs in the nBG group were brushed with nBG suspensions for 20 s. RGDS (GenScript, Nanjing, China) peptide was synthesized and labeled by covalently binding fluorescein isothiocyanate (FITC) to the N-terminus of the amino acid. The molecular formula of RGDS is $C_{15}H_{27}N_7O_8$, and the structural formula is shown in Fig. 1D. The purity is 98.5 %. The molecular weight of RGDS is 433.42, and the isoelectric point is approximately 6.3. RGDS peptide was added to 1 mM HEPES (pH = 7.0) to prepare a 100 μM RGDS solution. The dentin discs in the RGDS group were incubated in RGDS solution at a ratio of 10 μl/mm^3 for 2 h and then washed with deionized water 3–5 times to remove excess peptides. The amount of RGDS in the supernatant solution before and after incubation with
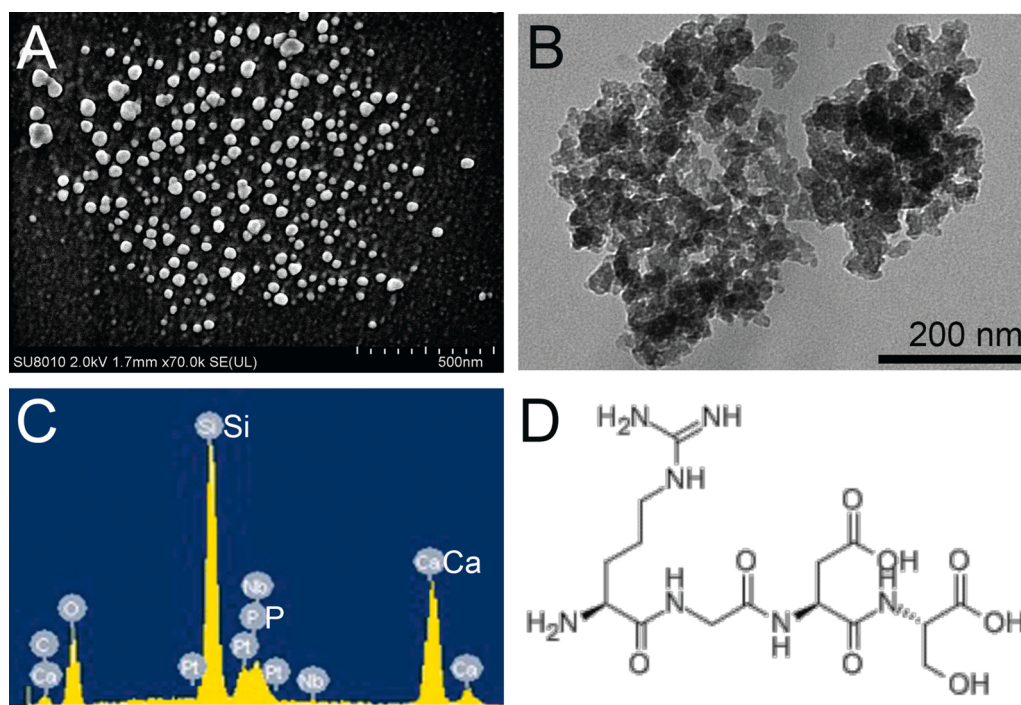
Fig. 1. Characteristics of nBG and RGDS.
Morphology of nBG determined by SEM (A) and TEM (B); (C) Surface elemental composition of nBG determined by EDS; (D) Structural formula of RGDS.

dentin discs was determined by BCA protein assay. The dentin discs that were incubated in RGDS for 2 h and then treated with nBG particles formed the RGDS + nBG group. All specimens were stored in individual stimulated body fluid (SBF) containers for 2 weeks at 37 °C for remineralization [31], and the SBF solution was changed every 24 h.

2.3. Field emission scanning electron microscopy (FE-SEM)

RGDS- and/or nBG-treated dentin disks were prepared as previously described and observed under FE-SEM (S4800; JEOL, Tokyo, Japan) (n = 8). Eight additional specimens in each of the control, RGDS, nBG, and RGDS + nBG groups were incubated in SBF for 2 weeks to observe mineral formation on dentin by FE-SEM. All specimens were dried at 60 °C for three days, coated with a 15 nm layer of Pt/Pd to increase the conductivity, and then examined using FE-SEM. The surface elemental compositions were evaluated using an energy-dispersive X-ray spectroscopy (EDS) and FE-SEM.

2.4. X-ray diffraction (XRD)

XRD analysis was carried out before and after 2 weeks of remineralization for specimens in the control, RGDS, nBG, and RGDS + nBG groups (n = 8). The specimens were dried at 60 °C for three days before testing. XRD spectra were collected using a Rigaku (D/MAX 2500, Rigaku, Japan) instrument with Cu Kα (λ =1.54 Å) operated at 40 kV and 200 mA. Data were collected for 2θ values between 10° and 70° with a speed of 4°/min.

2.5. Confocal laser scanning microscopy

RGDS- and/or nBG-treated dentin disks were prepared as previously described and observed under a confocal laser scanning microscope (FV1000; Olympus, Tokyo, Japan) (n = 8). Eight additional specimens in each of the control, RGDS, nBG, and RGDS + nBG groups were incubated in SBF for 2 weeks to observe mineral formation on dentin by confocal microscopy. All specimens were observed under a confocal laser scanning microscope (FV1000; Olympus, Tokyo, Japan). Fluorescence images were obtained with a 1-µm z-step to optically section the specimens to a maximum depth of 15 µm below the dentin surface. The configuration of the system was standardized and used at the same setting for different groups.

2.6. Transmission electron microscopy (TEM)

Specimens in the control, RGDS, nBG, and RGDS + nBG groups were incubated in SBF for 2 weeks (n = 4) fixed with 10 % formalin, dehydrated in graded ethanol, and embedded in epoxy resin. Sections with a thickness of 70 nm were cut from resin blocks using an ultramicrotome (UC6, Leica, Germany) and then double stained with 2% uranyl acetate and lead citrate. The formation of the minerals in the samples was observed by TEM (Tecnai G2 F30, FEI, USA).

2.7. Dentin cohesive strength

Dentin discs at the crown part of the teeth were cut at a thickness of 1 mm with a hard histotome. The orientation of the tubule was cut perpendicular to the dentin surface. Dentin discs were then cut into dentin sticks with a length, height and width of 8 mm, 1 mm and 1 mm, respectively. The dentin sticks were randomly divided into control, RGDS, nBG, and RGDS + nBG groups (n = 20). The entire surface of each dentin stick was brushed with nBG suspension or/and incubated with RGDS. All specimens were then incubated in SBF for 2 weeks, rinsed with deionized water for 20 s, and dried at room temperature for 2 min. The specimens were submitted to a dentin cohesive strength test in a microtensile tester (T-61,010 K, Bisco, USA) at a crosshead speed of 0.5 mm/min. The maximum load p(N) was recorded, and the dentin

cohesive strength σt (MPa) was calculated according to the following formula: $\sigma t = p/(b \times d)$, where b is the sample width (1 mm) and d is the sample thickness (1 mm).

The dentin cohesive strength data were analyzed using SPSS version 21 (SPSS Inc., IL, USA). Homogeneity of variance was determined using Levene's test. Normal distribution of data was assessed using the Shapiro-Wilk test. One-way ANOVA and Tukey's test were employed to determine the differences. The value of each group is expressed as the mean $\pm$ standard deviation (SD). $P < 0.05$ was considered statistically significant.

2.8. Mineralization of type I collagen fibrils

Self-assembled collagen fibrils were prepared as reported [32]. A single layer of type I collagen fibrils was reconstituted over formvar- and carbon-coated 400 mesh Ni TEM grids (Zhongjingkeyi, P. R. China) by neutralizing a 0.1 mg/mL collagen stock solution (pH 4–5) with 1 mol/L NaOH. To prepare the collagen stock solution, 100 µL of lyophilized type I collagen powder derived from rat tails (Corning, New York, NY, USA) was dissolved in 300 µL of acetic acid (0.1 mol/L and pH 3.0) and 400 µL of potassium solution that contained KCl (200 mmol/L), Na_2HPO_4 (30 mmol/L), and KH_2PO_4 (10 mmol/L). The neutralized collagen solution was left to gel by incubating at 37 °C for a maximum of 24 h. To stabilize the structure of the reconstituted collagen fibrils, collagen cross-linking was carried out using 0.3 mol/L 1-ethyl-3-(3-(dimethylamino)propyl)-carbodiimide (Sigma-Aldrich, St. Louis, MO, USA) and 0.06 mol/L N-hydroxysuccinimide (Sigma-Aldrich, USA) for 4 h. Thereafter, the collagen-coated grids were briefly immersed in deionized water and then dried in air. The collagen-coated grids were placed upside down over 100 µL SBF containing 100 µM RGDS and/or 0.5 g/mL nBG inside a 100 % humidity chamber for 72 h. The control group utilized 100 µl SBF. The collagen-coated grids were then washed with deionized water, dried in air, and observed with TEM.

3. Results

3.1. Attachment of RGDS and/or nBG on demineralized dentin discs

The amount of RGDS adsorbed on the dentin discs was determined by measuring the depletion in the supernatant solution prior to and after adsorption. Before and after incubating RGDS with the dentin discs, the amount of RGDS in the solution was 32.88 $\pm$ 5.84 ng/µl and 7.71 $\pm$ 3.04 ng/µl, respectively, indicating that approximately 80 % of the RGDS in the solution was adsorbed on the dentin discs (Fig. 2A). No release of RGDS from dentin was detected during 2 weeks of immersion in SBF.

SEM and EDS were used to observe the attachment and distribution of nBG on the demineralized dentin. After demineralization by EDTA, the dentinal tubules were completely open, and collagen fibrils around the dentinal tubules in the control group and RGDS group were exposed (Fig. 2B,C,E,F). The yellow arrows in Fig. 2C and F represent collagen fibrils. No silicon element was detected on the surface of untreated and RGDS-treated dentin by EDS (Fig. 2D, G). After treating the specimens with nBG, the nBG particles adhered to the dentinal collagen fibrils (Fig. 2H,I), and some silicon was detected on the dentin surface, indicating the presence of nBG on dentin (Fig. 2J). As indicated by silicon, more nBG particles adhered to RGDS + nBG-treated dentin than to nBG-treated dentin, and the collagen fibrils were completely covered by attached particles and were no longer shown (Fig. 2K,L,M). The yellow arrowheads in Fig. 2I and L represent nBG particles.

There were no obvious diffraction peaks in the XRD patterns of the samples in all groups, indicating that the dentin surface was completely demineralized (Fig. 2N).

Confocal immunofluorescence was used to further detect the attachment of RGDS and nBG on demineralized dentin. RGDS peptide labeled with FITC produced green fluorescence, and the nBG particles
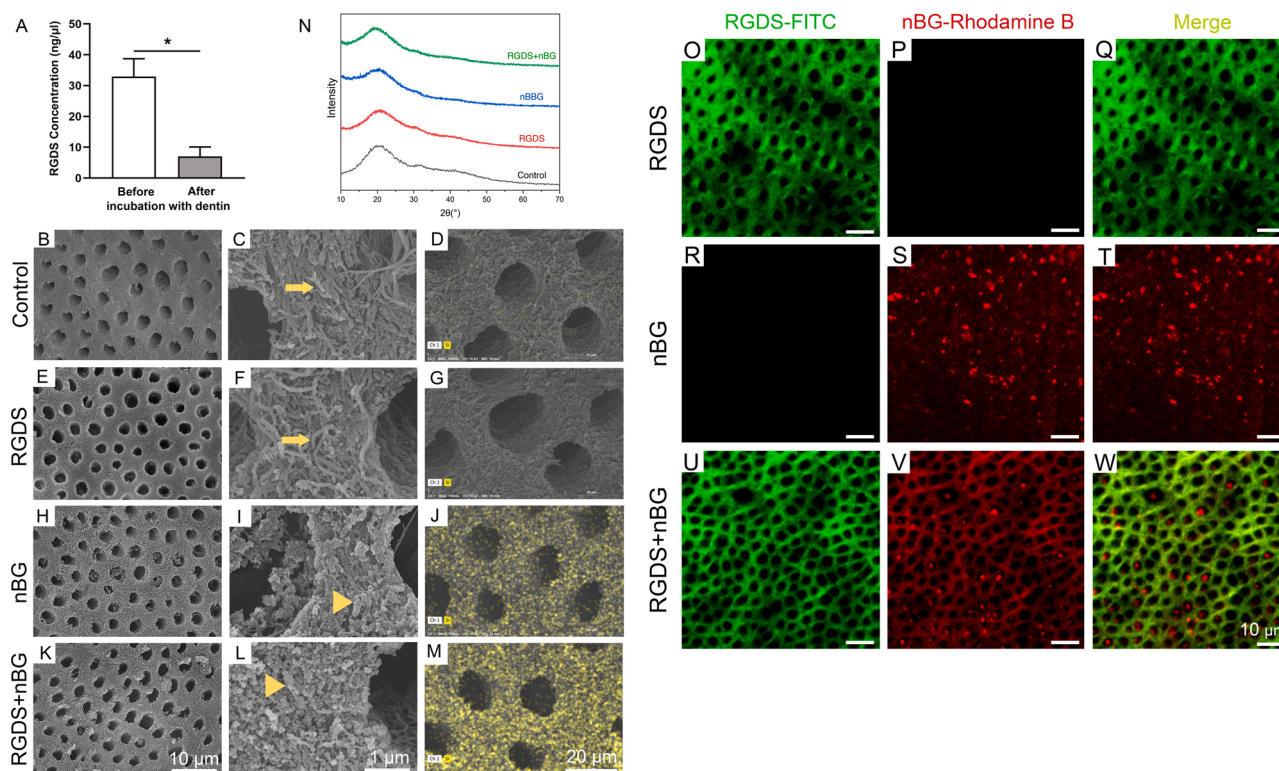
Fig. 2. Demineralized dentin discs immediately following different treatments.
A: RGDS depletion in supernatant solution prior to and after adsorption to dentin; SEM and EDS for silicon of untreated dentin (B,C,D), RGDS-treated dentin (E,F,G), nBG-treated dentin (H,I,J) and RGDS + nBG-treated dentin (K,L,M). The yellow arrow represents collagen fibrils, and the yellow arrowhead represents nBG particles. N: XDR spectra of untreated dentin (black), RGDS-treated dentin (red), nBG-treated dentin (blue) and RGDS + nBG-treated dentin (green). Confocal immunofluorescence images of RGDS-treated dentin (O,P,Q), nBG-treated dentin (R,S,T) and RGDS + nBG-treated dentin (U,V,W). RGDS appears green; nBG appears red; and RGDS and nBG colocalization appears yellow.

labeled with rhodamine B produced red fluorescence. Because the RGDS with green fluorescence was adsorbed homogeneously onto the dentin of the RGDS group, the outline of the dentinal tubules was clearly shown (Fig. 2O-Q). Scattered and aggregated nBG particles were detected on the surface of the nBG-treated dentin, but no dentin tubule structure was observed, indicating that part of the dentin surface was not covered by nBG particles (Fig. 2R-T). For the RGDS + nBG group, both RGDS and nBG were observed on the entire surface of the dentin. Compared with that of the nBG group, the red fluorescence area of the RGDS + nBG group was larger, and the structure of the dentin tubules was outlined by red fluorescence, indicating that more nBG particles were adsorbed on RGDS + nBG-treated dentin (Fig. 2U-W).

3.2. Apatite formation on RGDS- and/or nBG-treated dentin after 2 weeks of remineralization

After the samples were incubated in SBF for 2 weeks, SEM showed that no minerals formed in the control and RGDS groups, and collagen fibrils were clearly shown (Fig. 3A-D). The yellow arrow in Fig. 3B and D represents the collagen fibrils. Minerals were formed on the dentin surface of the nBG and RGDS + nBG groups (Fig. 3E-H). Some dentin tubules were covered by the newly formed minerals in the nBG group. Almost completely sealed tubules can be detected in the RGDS + nBG-treated dentin discs. The yellow arrowhead in Fig. 3F and H represents the newly formed minerals.

The form of apatite on nBG-treated dentin and RGDS + nBG-treated dentin was evident from the XRD spectra, intensified diffraction peaks (26° and 32°) which indicated HA were noted after 2 weeks of remineralization (Fig. 3I). There were no obvious diffraction peaks in the XRD patterns of the samples in the control and RGDS groups.

Confocal immunofluorescence was used to further observe apatite

formation in the dentinal tubules. After incubating in the SBF for 2 weeks, no apatite formation was observed in the RGDS group, while confocal imaging revealed the presence of RGDS in the dentin specimens because it fluoresced green (Fig. 3J-M). Specimens in the nBG and RGDS + nBG groups showed the formation of distinctive rod-like apatite that adapted to the dentin tubules (Fig. 3N-U). In particular, red-fluorescent minerals in the RGDS + nBG group were associated with green-fluorescent peritubular dentin (Fig. 3U), indicating that RGDS-mediated nBG not only promoted apatite formation but also may have induced the remineralization of peritubular dentin. The maximum depth of the apatite rod was measured from the dentin surface to the tip of the apatite rod, where fluorescence was no longer detectable. The 3D reconstruction images showed that the maximum depth of the newly formed apatite rods in the nBG group was 8 μm, while the apatite rods in the RGDS + nBG group were thicker and extended into the tubules to a maximum depth of 12 μm (Fig. 3V-X).

3.2. Remineralization of the treated dentin matrix

Dentin remineralization in different groups was observed by TEM. The deeply stained area in the field of view represents the mineralized area, and the collagen appears as light gray strips. After incubating in SBF for 2 weeks, dentinal tubules and collagen structures were observed in the experimental groups and the control group at low magnification (Fig. 4A, D, G and J). The high-magnification field showed no mineral deposition in and between the collagens in the control and RGDS groups, and the collagen profile was distinct (Fig. 4B and E). Specimens in the nBG and RGDS + nBG groups showed deeply stained mineralized areas, and the collagen profile was not distinct (Fig. 4H and K). At increased magnification, a large amount of crystal lattice formation was observed in the dentin samples in the nBG group and RGDS + nBG group (Fig. 4I
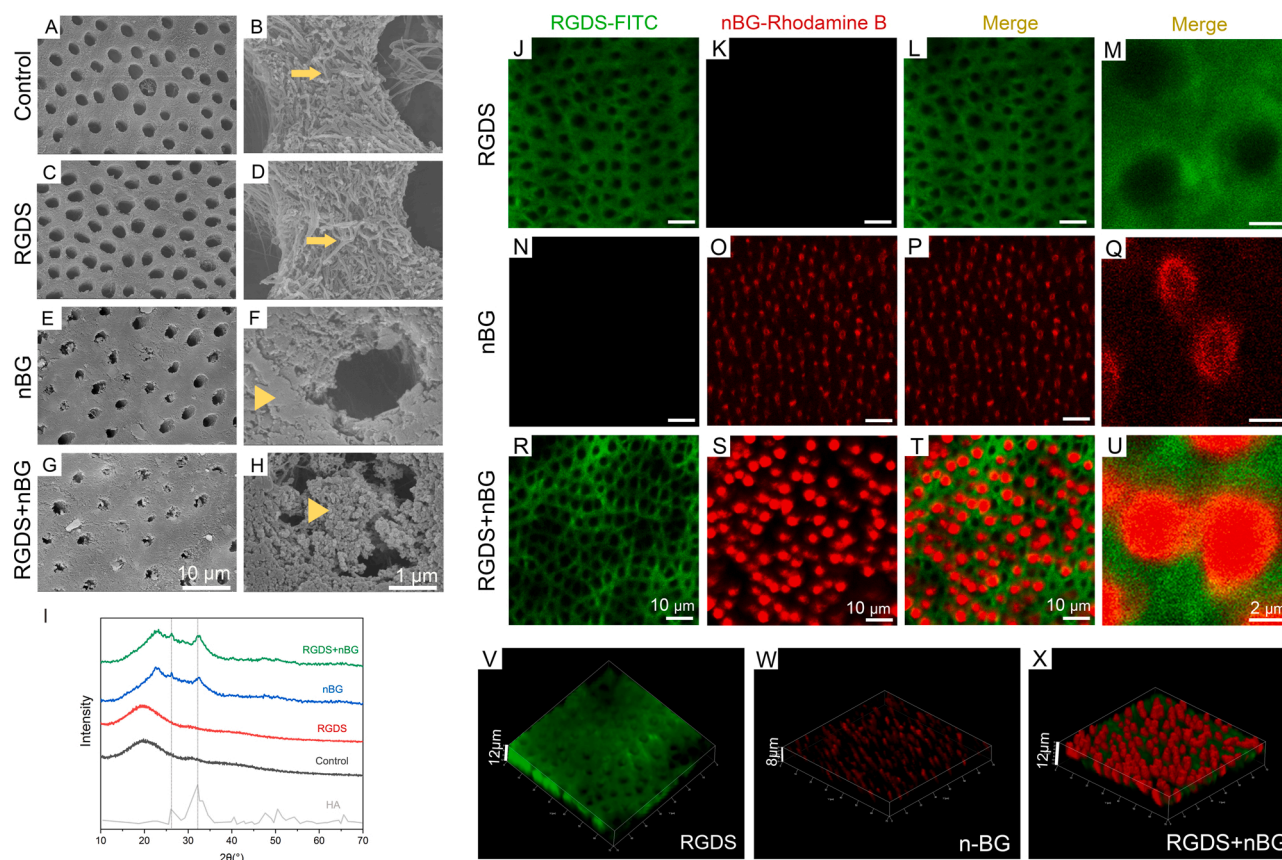
Fig. 3. Apatite formation on dentin with different treatments after 2 weeks of remineralization.
SEM of untreated dentin (A,B), RGDS-treated dentin (C,D), nBG-treated dentin (E,F) and RGDS + nBG-treated dentin (G,H). The yellow arrow represents the collagen fibrils, and the yellow arrowhead represents the newly formed minerals. I: XDR spectra of HA, untreated dentin (black), RGDS-treated dentin (red), nBG-treated dentin (blue) and RGDS + nBG-treated dentin (green). Confocal immunofluorescence images of RGDS-treated dentin (J,K,L,M), nBG-treated dentin (N,O,P,Q) and RGDS + nBG-treated dentin (R,S,T,U). 3D reconstruction of immunofluorescence images of RGDS-treated dentin (V), nBG-treated dentin (W) and RGDS + nBG-treated dentin (X). RGDS appears green, nBG appears red, and RGDS and nBG colocalization appears yellow.

and L), while the control and RGDS groups had no crystal lattice formation (Fig. 4C and F). The inserted SEAD images showed that the dentin samples of the nBG group and RGDS + nBG group had stronger diffused rings than those of the RGDS and control groups, but there was no obvious diffraction ring in all groups. These results indicated that although minerals may be formed in nBG- and RGDS + nBG-treated dentin, the mineral content may be low.

3.3. Dentin cohesive strength of the treated dentin

According to the Shapiro-Wilk test, the dentin cohesive strength data were normally distributed ($P > 0.05$). The dentin cohesive strength of the nBG-treated dentin (31.02 ± 2.30 MPa) and RGDS + nBG-treated dentin (33.71 ± 2.82 MPa) was significantly higher than that in the control group (22.83 ± 2.18 MPa) and RGDS group (22.67 ± 2.26 MPa) ($P<0.05$). The specimens in the RGDS + nBG group had the highest dentin cohesive strength among the samples tested herein ($P < 0.05$) (Fig. 5A).

3.4. Mineralization of type I collagen fibrils

A single layer of self-assembled type I collagen fibrils was used to evaluate the mineralization effect of RGDS and nBG. After reacting with SBF for 3 days, the collagen fibrils in the control group and in the RGDS group exhibited smooth edges and specific periodic stripes, which consisted of gaps and overlapping zones (Fig. 5B,C), indicating that no mineralization was formed. Collagen fibrils exposed to nBG and

RGDS + nBG exhibited minerals (white arrow in Fig. 5D,E) inside the collagen fibrils. The stripes of collagen could no longer be observed by TEM.

4. Discussion

This study showed that nBG, especially in association with RGDS, was able to form an apatite layer on the dentin surface and apatite rods in the dentinal tubules. Apatite growth involves multiple axes; the apatite that grew along the c-axis formed needle-like crystallites, while the apatite that grew along the *a*-axis formed platelet-like crystallites [33,34]. The orientation and development of the apatite crystallites is controlled by the interdiffusion kinetics and diffusion direction of the ions at the propagating interface [35]. This finding suggested that apatite formation may be affected by the distribution of BG on the dentin and the structural characteristics of the dentin. After BG was attached to the dentin surface, it underwent dissolution and formed an apatite layer [36]. In contrast, the formation of apatite with a rod-like structure may be constrained by the dentinal tubules, and the local ion diffusion gradient in the dentinal tubules is more likely to enhance the directional crystallization and continuous expansion of the apatite at the tips of the rods [37]. The nBG particles with a size of 20 nm became lodged within the dentinal tubules, which may favor the formation of apatite rods, and the nanoBGs led to rapid apatite formation due to their smaller size and larger surface area [38]. RGDS improved nBG-induced apatite formation, which occluded more dentinal tubules and had deeper rod-like apatite in the dentinal tubules. This characteristic is beneficial to
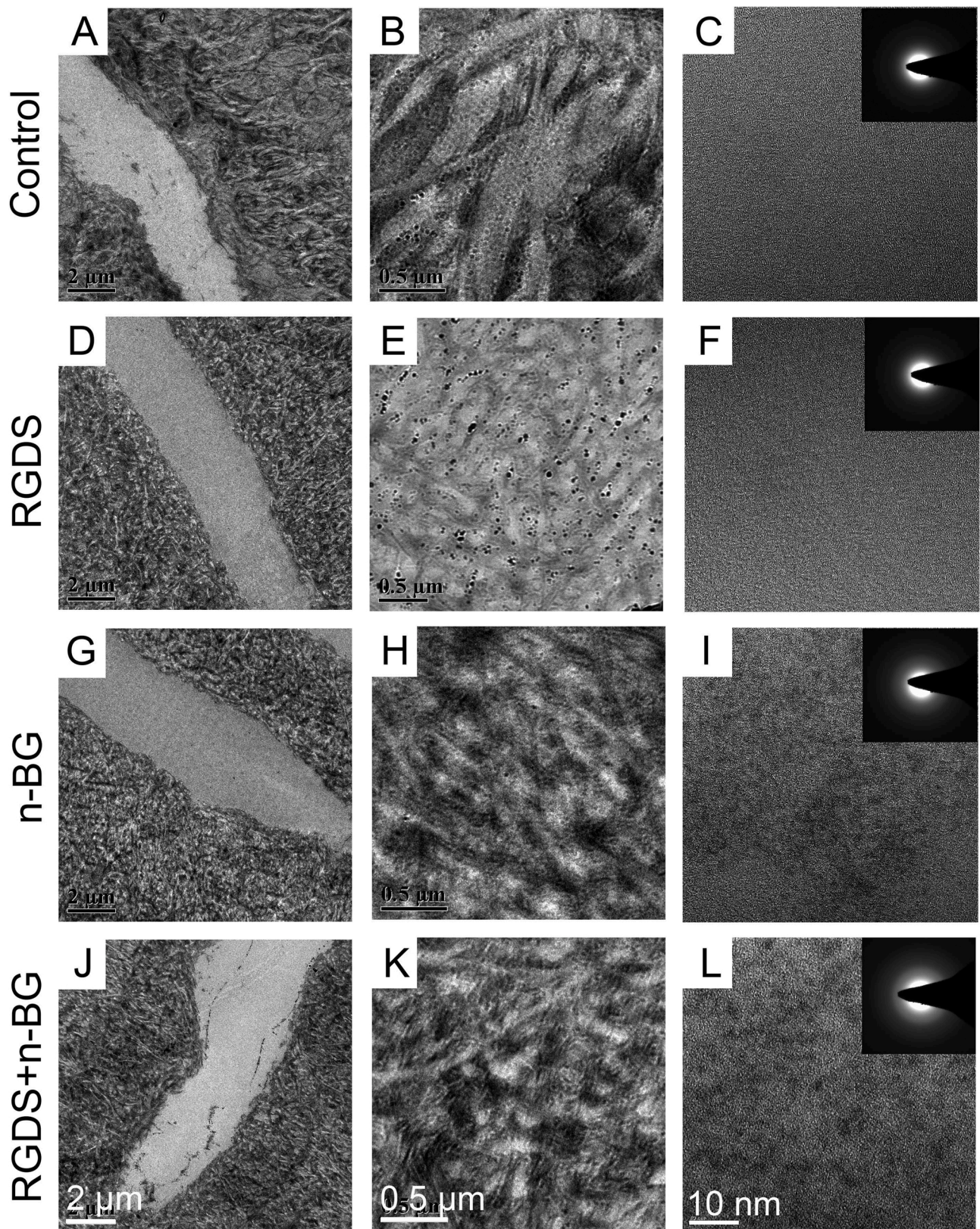
Fig. 4. TEM and SEAD images showing dentin remineralization.
Dentin specimens with different treatments incubated in SBF for two weeks. A-C: Untreated dentin; D-F: RGDS-treated dentin; G-I: nBG-treated dentin; and J-L: RGDS + nBG-treated dentin.
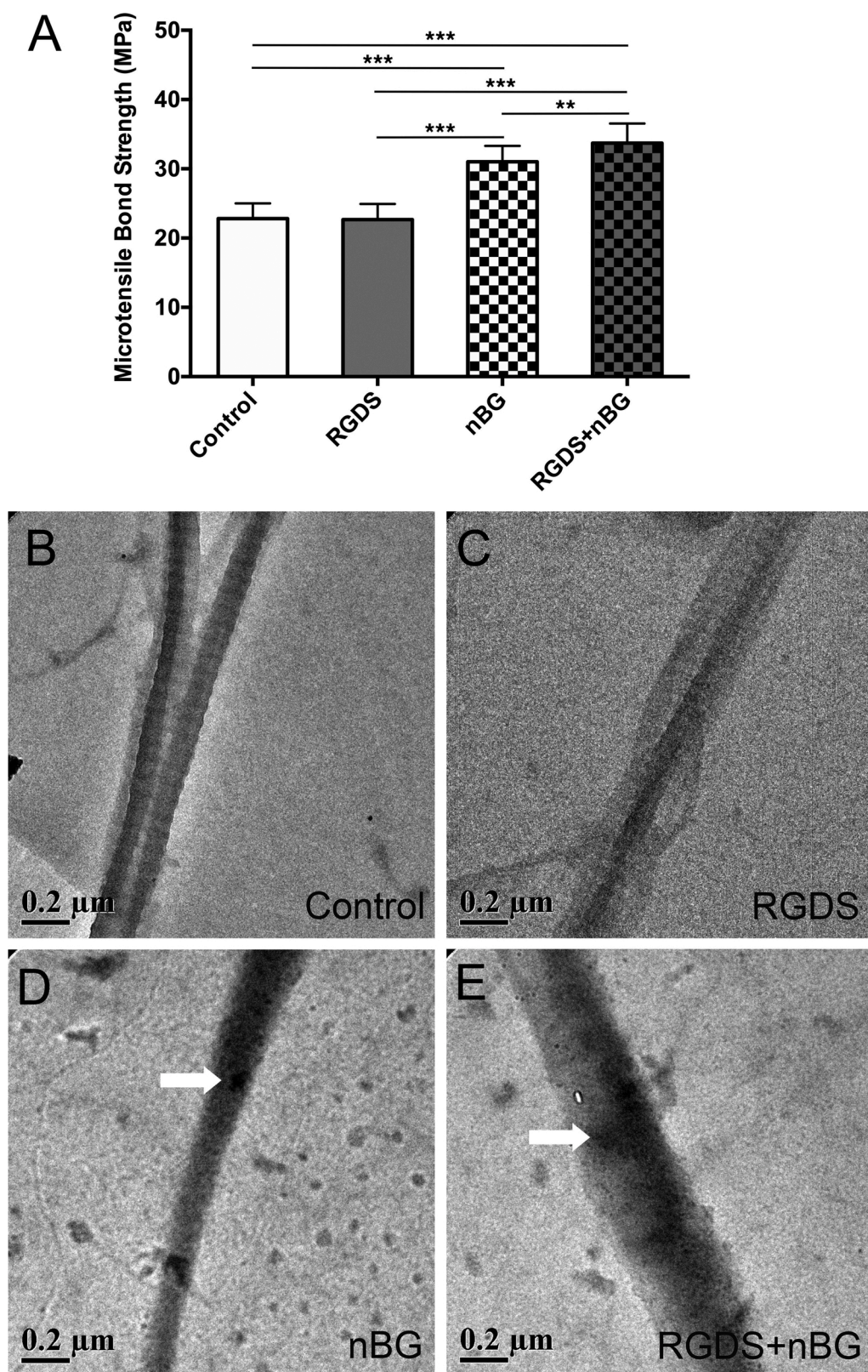
Fig. 5. Dentin cohesive strength and collagen mineralization with different treatments.
A: Dentin cohesive strength of treated dentin specimens. * indicates statistical significance, $P < 0.05$; ** indicates statistical significance, $P < 0.01$; *** indicates statistical significance, $P < 0.001$. Transmission electron microscopy images of untreated type I collagen fibrils (B), type I collagen fibrils treated with RGDS (C), nBG (D), and RGDS + nBG (E) for 3 days. The white arrow represents the newly formed minerals.

improving the treatment effect and stability of dentin hypersensitivity and dental erosion.

The key to restoring demineralized dentin is to mineralize the dentin collagen matrix, not just to form minerals on the surface of dentin. In this study, nBG also induced crystal formation in the demineralized dentin matrix and further improved the dentin cohesive strength, which indicated that mineral crystallites were closely linked or even chemically bound to the collagen matrix. BGs have been proposed for dentin remineralization because they provide calcium and phosphate ions. Vollenweider et al. found that dentin treated with 20–50 nm BG nanoparticles had a pronounced increase in mineral content, suggesting rapid remineralization. However, the lack of mechanical reconstitution of the

remineralized dentin sample indicated an imperfect arrangement of the newly deposited mineral [39]. A recent study suggested that the use of BG increased root dentin microhardness [16]. Nanoparticles have the ability to penetrate dentin and remain embedded within the collagen matrix, and then the infiltrated particles may release ions and nuclei for mineral growth in dentin [40].

In the biomineralization process, NCPs are bound to the collagen matrix and play an important role in controlling apatite nucleation and growth. Using confocal laser scanning microscopy and SEM analysis, our results demonstrated that the RGDS peptide was able to bind to dentin collagen, captured more nBG particles than the untreated dentin and further promoted HA nucleation and growth. It has been reported that more metastable amorphous calcium phosphate (ACP) nanoprecursors were combined with the collagen matrix in demineralized dentin pre-incubated with peptides in phosphate-containing fluid than in dentin without peptide treatment [21]. RGDS is negatively charged and may be able to adsorb positively charged calcium ions, which further combine with phosphate ions to form ACP [41]. Aspartic acid can increase ion supersaturation in localized regions in the solution and inhibit calcium phosphate crystallization [42,43]. Aspartic acid and serine can combine with special sites on the collagen surface to guide calcium phosphate into collagen fibers [42,44]. A recent study found that aspartic acid promoted the crystallization kinetics of metastable ACP to hydroxyapatite, promoted the biomimetic remineralization of demineralized dentin and shortened the remineralization time [45]. Therefore, the aspartic acid and serine in RGDS may contribute to its induction of dentin remineralization. Furthermore, dentin repair or regeneration can be achieved by stimulating odontoblasts or stem/progenitor cells, secreting reactionary or reparative dentin. Our previous studies confirmed that BGs induce odontogenesis and promote dentin formation [29,46]. The RGDS peptide is known to improve cell adhesion [47,48]. Therefore, in the presence of cells, due to the bioactivity of both RGDS and nBG, nBG mediated by RGDS may also provide satisfactory cell and tissue reactions.

5. Conclusions

RGDS could bind to dentin and enhance the attachment of nBG. RGDS-mediated nBG effectively enhanced dentin remineralization and improved dentin cohesive strength. The results presented here introduce a wide array of applications in dentin erosion, dentin hypersensitivity, dentin bonding interface improvement, and regenerative dentistry. Further research is needed to obtain the optimal concentration and processing time of nBG and RGDS and to investigate how the RGDS behaves during dentin remineralization.

CRediT authorship contribution statement

Sainan Wang: Conceptualization, Methodology, Visualization, Writing - original draft, Funding acquisition. **Xuyan Sheng:** Investigation, Formal analysis, Visualization. **Guibin Huang:** Investigation, Formal analysis, Visualization. **Qiuju Li:** Investigation, Visualization. **Yanmei Dong:** Conceptualization, Supervision, Writing - review & editing, Funding acquisition.

Declaration of Competing Interest

The authors report no declarations of interest.

Acknowledgements

References

[1] L. Breschi, A. Mazzoni, A. Ruggeri, M. Cadenaro, R. Di Lenarda, E. De Stefano Dorigo, Dental adhesion review: aging and stability of the bonded interface, Dent. Mater. 24 (1) (2008) 90–101, https://doi.org/10.1016/j.dental.2007.02.009.

[2] W. Zhou, S. Liu, X. Zhou, M. Hannig, S. Rupf, J. Feng, X. Peng, L. Cheng, Modifying adhesive materials to improve the longevity of resinous restorations, Int. J. Mol. Sci. 20 (3) (2019), https://doi.org/10.3390/ijms20030723.

[3] S.K. Jun, S.A. Yang, Y.J. Kim, A. El-Fiqi, N. Mandakhbayar, D.S. Kim, J. Roh, S. Sauro, H.W. Kim, J.H. Lee, H.H. Lee, Multi-functional nano-adhesive releasing therapeutic ions for MMP-deactivation and remineralization, Sci. Rep. 8 (1) (2018) 5663, https://doi.org/10.1038/s41598-018-23939-6.

[4] I.M. Garcia, V.C.B. Leitune, S.M.W. Samuel, F.M. Collares, Influence of different calcium phosphates on an experimental adhesive resin, J. Adhes. Dent. 19 (5) (2017) 379–384, https://doi.org/10.3290/j.jad.a38997.

[5] W.J. Landis, K.J. Hodgens, J. Arena, M.J. Song, B.F. McEwen, Structural relations between collagen and mineral in bone as determined by high voltage electron microscopic tomography, Microsc. Res. Tech. 33 (2) (1996) 192–202.

[6] L.E. Bertassoni, S. Habelitz, J.H. Kinney, S.J. Marshall, G.W. Marshall Jr., Biomechanical perspective on the remineralization of dentin, Caries Res. 43 (1) (2009) 70–77, https://doi.org/10.1159/000201593.

[7] J.H. Kinney, S. Habelitz, S.J. Marshall, G.W. Marshall, The importance of intrafibrillar mineralization of collagen on the mechanical properties of dentin, J. Dent. Res. 82 (12) (2003) 957–961, https://doi.org/10.1177/154405910308201204.

[8] C.Y. Cao, M.L. Mei, Q.L. Li, E.C. Lo, C.H. Chu, Methods for biomimetic remineralization of human dentine: a systematic review, Int. J. Mol. Sci. 16 (3) (2015) 4615–4627, https://doi.org/10.3390/ijms16034615.

[9] A.K. Burwell, L.J. Litkowski, D.C. Greenspan, Calcium sodium phosphosilicate (NovaMin): remineralization potential, Adv. Dent. Res. 21 (1) (2009) 35–39, https://doi.org/10.1177/0895937409335621.

[10] X. Liu, V. Barnes, W. DeVizio, H. Yang, H. Malmstrom, Y. Ren, Effects of dentin tubule occlusion by dentifrice containing a PVM/MA bioadhesive copolymer in a silica base, J. Dent. 39 (4) (2011) 293–301, https://doi.org/10.1016/j.jdent.2010.10.016.

[11] A.P. Forsback, S. Areva, J.I. Salonen, Mineralization of dentin induced by treatment with bioactive glass S53P4 in vitro, Acta Odontol. Scand. 62 (1) (2004) 14–20, https://doi.org/10.1080/00016350310008012.

[12] B.S. Lee, S.H. Kang, Y.L. Wang, F.H. Lin, C.P. Lin, In vitro study of dentinal tubule occlusion with sol-gel DP-bioglass for treatment of dentin hypersensitivity, Dent. Mater. J. 26 (1) (2007) 52–61, https://doi.org/10.4012/dmj.26.52.

[13] M.R. Syed, M. Khan, F. Sefat, Z. Khurshid, M.S. Zafar, A.S. Khan, Bioactive glass and glass fiber composite: biomedical/dental applications, Biomedical, Therapeutic and Clinical Applications of Bioactive Glasses (2019) 467–495. Elsevier.

[14] J.H. Jang, M.G. Lee, J.L. Ferracane, H. Davis, H.E. Bae, D. Choi, D.S. Kim, Effect of bioactive glass-containing resin composite on dentin remineralization, J. Dent. 75 (2018) 58–64, https://doi.org/10.1016/j.jdent.2018.05.017.

[15] F. Schwendicke, A. Al-Abdi, A. Pascual Moscardo, A. Ferrando Cascales, S. Sauro, Remineralization effects of conventional and experimental ion-releasing materials in chemically or bacterially-induced dentin caries lesions, Dent. Mater. 35 (5) (2019) 772–779, https://doi.org/10.1016/j.dental.2019.02.021.

[16] O. Santos Cardoso, M. Coelho Ferreira, E. Moreno Carvalho, P.V. Campos Ferreira, J. Bauer, C.N. Carvalho, Effect of root repair materials and bioactive glasses on microhardness of dentin, Iran. Endod. J. 13 (3) (2018) 337–341, https://doi.org/10.22037/iej.v13i3.20565.

[17] X.-Y. Sheng, W.-Y. Gong, Q. Hu, X.-f. Chen, Y.-M. Dong, Mineral formation on dentin induced by nano-bioactive glass, Chinese Chem. Lett. 27 (9) (2016) 1509–1514, https://doi.org/10.1016/j.cclet.2016.03.030.

[18] G. He, S. Gajjeraman, D. Schultz, D. Cookson, C. Qin, W.T. Butler, J. Hao, A. George, Spatially and temporally controlled biomineralization is facilitated by interaction between self-assembled dentin matrix protein 1 and calcium phosphate nuclei in solution, Biochemistry 44 (49) (2005) 16140–16148, https://doi.org/10.1021/bi051045l.

[19] L.W. Fisher, DMP1 and DSPP: evidence for duplication and convergent evolution of two SIBLING proteins, Cells Tissues Organs (Print) 194 (2-4) (2011) 113–118, https://doi.org/10.1159/000324254.

[20] Y. Cao, W. Liu, T. Ning, M.L. Mei, Q.L. Li, E.C. Lo, C.H. Chu, A novel oligopeptide simulating dentine matrix protein 1 for biomimetic mineralization of dentine, Clin. Oral Investig. 18 (3) (2014) 873–881, https://doi.org/10.1007/s00784-013-1035-y.

[21] Q. Wang, X. Wang, L. Tian, Z. Cheng, F. Cui, In situ remineralizaiton of partially demineralized human dentine mediated by a biomimetic non-collagen peptide, Soft Matter 7 (20) (2011) 9673–9680.

[22] Y.C. Chien, J. Tao, K. Saeki, A.F. Chin, J.L. Lau, C.L. Chen, R.N. Zuckermann, S.J. Marshall, G.W. Marshall, J.J. De Yoreo, Using biomimetic polymers in place of noncollagenous proteins to achieve functional remineralization of dentin tissues, ACS Biomater. Sci. Eng. 3 (12) (2017) 3469–3479, https://doi.org/10.1021/acsbiomaterials.7b00378.

[23] M. Bacino, V. Girn, H. Nurrohman, K. Saeki, S.J. Marshall, L. Gower, E. Saeed, R. Stewart, T. Le, G.W. Marshall, S. Habelitz, Integrating the PILP-mineralization process into a restorative dental treatment, Dent. Mater. 35 (1) (2019) 53–63, https://doi.org/10.1016/j.dental.2018.11.030.

[24] N. Saxena, M.A. Cremer, E.S. Dolling, H. Nurrohman, S. Habelitz, G.W. Marshall, L. B. Gower, Influence of fluoride on the mineralization of collagen via the polymer-induced liquid-precursor (PILP) process, Dent. Mater. 34 (9) (2018) 1378–1390, https://doi.org/10.1016/j.dental.2018.06.020.

[25] G. He, T. Dahl, A. Veis, A. George, Dentin matrix protein 1 initiates hydroxyapatite formation in vitro, Connect. Tissue Res. 44 (Suppl 1) (2003) 240–245.

[26] C. Qin, R. D'Souza, J.Q. Feng, Dentin matrix protein 1 (DMP1): new and important roles for biomineralization and phosphate homeostasis, J. Dent. Res. 86 (12) (2007) 1134–1141, https://doi.org/10.1177/154405910708601202.

[27] F.-Z. Cui, Y. Li, J. Ge, Self-assembly of mineralized collagen composites, Mater. Sci. Eng. R Rep. 57 (1-6) (2007) 1–27.

[28] A. Shrestha, S. Friedman, A. Kishen, Photodynamically crosslinked and chitosan-incorporated dentin collagen, J. Dent. Res. 90 (11) (2011) 1346–1351, https://doi.org/10.1177/0022034511421928.

[29] S. Wang, X. Gao, W. Gong, Z. Zhang, X. Chen, Y. Dong, Odontogenic differentiation and dentin formation of dental pulp cells under nanobioactive glass induction, Acta Biomater. 10 (6) (2014) 2792–2803, https://doi.org/10.1016/j.actbio.2014.02.013.

[30] L. Xu, S. Gao, R. Zhou, F. Zhou, Y. Qiao, D. Qiu, Bioactive pore-forming bone adhesives facilitating cell ingrowth for fracture healing, Adv Mater 32 (10) (2020) e1907491, https://doi.org/10.1002/adma.201907491.

[31] T. Kokubo, H. Kushitani, S. Sakka, T. Kitsugi, T. Yamamuro, Solutions able to reproduce in vivo surface-structure changes in bioactive glass-ceramic A-W, J. Biomed. Mater. Res. 24 (6) (1990) 721–734, https://doi.org/10.1002/jbm.820240607.

[32] Y. Liu, Y.K. Kim, L. Dai, N. Li, S.O. Khan, D.H. Pashley, F.R. Tay, Hierarchical and non-hierarchical mineralisation of collagen, Biomaterials 32 (5) (2011) 1291–1300, https://doi.org/10.1016/j.biomaterials.2010.10.018.

[33] C. Shao, B. Jin, Z. Mu, H. Lu, Y. Zhao, Z. Wu, L. Yan, Z. Zhang, Y. Zhou, H. Pan, Z. Liu, R. Tang, Repair of tooth enamel by a biomimetic mineralization frontier ensuring epitaxial growth, Sci. Adv. 5 (8) (2019), https://doi.org/10.1126/sciadv.aaw9569 eaaw9569.

[34] K. Sato, Mechanism of hydroxyapatite mineralization in biological systems, J. Ceram. Soc. Jpn. 115 (1338) (2007) 124–130.

[35] S. Hayakawa, Y. Li, K. Tsuru, A. Osaka, E. Fujii, K. Kawabata, Preparation of nanometer-scale rod array of hydroxyapatite crystal, Acta Biomater. 5 (6) (2009) 2152–2160, https://doi.org/10.1016/j.actbio.2009.02.018.

[36] L.L. Hench, H.A. Paschall, Direct chemical bond of bioactive glass-ceramic materials to bone and muscle, J. Biomed. Mater. Res. 7 (3) (1973) 25–42, https://doi.org/10.1002/jbm.820070304.

[37] A.R. Curtis, N.X. West, B. Su, Synthesis of nanobioglass and formation of apatite rods to occlude exposed dentine tubules and eliminate hypersensitivity, Acta Biomater. 6 (9) (2010) 3740–3746, https://doi.org/10.1016/j.actbio.2010.02.045.

[38] J.H. Jung, S.B. Park, K.H. Yoo, S.Y. Yoon, M.K. Bae, D.J. Lee, C.C. Ko, Y.H. Kwon, Y.I. Kim, Effect of different sizes of bioactive glass-coated mesoporous silica nanoparticles on dentinal tubule occlusion and mineralization, Clin. Oral Investig. 23 (5) (2019) 2129–2141, https://doi.org/10.1007/s00784-018-2658-9.

[39] M. Vollenweider, T.J. Brunner, S. Knecht, R.N. Grass, M. Zehnder, T. Imfeld, W. J. Stark, Remineralization of human dentin using ultrafine bioactive glass particles, Acta Biomater. 3 (6) (2007) 936–943, https://doi.org/10.1016/j.actbio.2007.04.003.

[40] A. Besinis, R. van Noort, N. Martin, Infiltration of demineralized dentin with silica and hydroxyapatite nanoparticles, Dent. Mater. 28 (9) (2012) 1012–1023, https://doi.org/10.1016/j.dental.2012.05.007.

[41] F. Nudelman, A.J. Lausch, N.A. Sommerdijk, E.D. Sone, In vitro models of collagen biomineralization, J. Struct. Biol. 183 (2) (2013) 258–269, https://doi.org/10.1016/j.jsb.2013.04.003.

[42] F. Nudelman, A.J. Lausch, N.A.J.M. Sommerdijk, E.D. Sone, In vitro models of collagen biomineralization, J. Struct. Biol. 183 (2) (2013) 258–269, https://doi.org/10.1016/j.jsb.2013.04.003.

[43] F. Nudelman, K. Pieterse, A. George, P.H. Bomans, H. Friedrich, L.J. Brylka, P. A. Hilbers, G. de With, N.A. Sommerdijk, The role of collagen in bone apatite formation in the presence of hydroxyapatite nucleation inhibitors, Nat. Mater. 9 (12) (2010) 1004–1009, https://doi.org/10.1038/nmat2875.

[44] L.-n. Niu, S.E. Jee, K. Jiao, L. Tonggu, M. Li, L. Wang, Y.-d. Yang, J.-h. Bian, L. Breschi, S.S. Jang, Collagen intrafibrillar mineralization as a result of the balance between osmotic equilibrium and electroneutrality, Nat. Mater. 16 (3) (2017) 370–378.

[45] L. Zhao, J. Sun, C. Zhang, C. Chen, Y. Chen, B. Zheng, H. Pan, C. Shao, B. Jin, R. Tang, X. Gu, Effect of aspartic acid on the crystallization kinetics of ACP and dentin remineralization, J. Mech. Behav. Biomed. Mater. 115 (2021) 104226, https://doi.org/10.1016/j.jmbbm.2020.104226.

[46] S. Wang, Q. Hu, X. Gao, Y. Dong, Characteristics and effects on dental pulp cells of a Polycaprolactone/Submicron bioactive glass composite scaffold, J. Endod. 42 (7) (2016) 1070–1075, https://doi.org/10.1016/j.joen.2016.04.023.

[47] M.I. Castellanos, C. Mas-Moruno, A. Grau, X. Serra-Picamal, X. Trepat, F. Albericio, M. Joner, F.J. Gil, M.P. Ginebra, J.M. Manero, Functionalization of CoCr surfaces with cell adhesive peptides to promote HUVECs adhesion and proliferation, Appl. Surf. Sci. 393 (2017) 82–92.

[48] B.K. Mann, J.L. West, Cell adhesion peptides alter smooth muscle cell adhesion, proliferation, migration, and matrix protein synthesis on modified surfaces and in polymer scaffolds, J. Biomed. Mater. Res. 60 (1) (2002) 86–93.